Applied Materials Today 29 (2022) 101639

Contents lists available at ScienceDirect

Applied Materials Today

journal homepage: www.elsevier.com/locate/apmt

Phase-transforming Ag-NiTi 3-D interpenetrating-phase composite with high recoverable strain, strength and electrical conductivity

Mingyang Zhang [a,b], Qin Yu [c,*], Huamiao Wang [d,*], Jian Zhang [a,e], Faheng Wang [a], Yining Zhang [a], Dake Xu [e], Zengqian Liu [a,b,**], Zhefeng Zhang [a,b,**], Robert O. Ritchie [c]

[a] Shi-Changxu Innovation Center for Advanced Materials, Institute of Metal Research, Chinese Academy of Sciences, Shenyang 110016, China
[b] School of Materials Science and Engineering, University of Science and Technology of China, Hefei 230026, China
[c] Department of Materials Science and Engineering, University of California Berkeley, Berkeley, CA 94720, USA
[d] State Key Laboratory of Mechanical System and Vibration, Shanghai Jiao Tong University, Shanghai 200240, China
[e] Shenyang National Laboratory for Materials Science, Northeastern University, Shenyang 110819, China

ARTICLE INFO

Keywords:
3-D interpenetrating-phase architecture
Elasticity
Nitinol
Composite
Electrical conductivity

ABSTRACT

It is of particular interest to achieve high elastic recoverable strain in the electrical contact materials while maintaining good electrical conductivity and decent tensile strength. It remains a challenge, especially for bulk-sized metallic materials, as the electrical conductivity and elastic strain limit (or tensile strength) are often mutually exclusive. Here, we present a material design strategy for overcoming this conflict by developing a Ag-NiTi composite with an interpenetrating-phase architecture via infiltrating Ag melt into the partially sintered porous NiTi scaffold. The composite exhibits a good combination of properties with high electrical conductivity comparable to metals, large elastic recoverable strain superior to most of bulk-sized conductive metals as well as higher tensile strength than most of alloys/composites based on silver and other noble metals. This new finding demonstrates that the interpenetrating-phase architecture design is promising for developing new materials for electrical contact application.

1. Introduction

Elasticity is an intrinsic property of materials that allows the deformed materials to restore their original configuration after external load is released provided that the internal stress/strain does not exceed the material's elastic limit. A high elasticity, *i.e.*, a relatively large elastic strain limit, is particularly appealing for electrical contact materials with regard to their electrical conductivity performance [1,2]. This is owing to the reality that the electrical resistance of electrical materials will be increased if the material undergoes excessive plastic deformation that produces crystal defects and structural damage [3–9]. Accordingly, achieving good electrical conductivity in electrical contact application requires a tight contact between the contact parts that experience mainly elastic deformation – this requests a large elastic strain limit of electrical contact materials. However, among various electrical contact materials, electrical conductivity and elasticity (or strength) are often mutually exclusive. Specifically, metallic materials that possess good conductivity usually exhibit small elastic strain limit (often less than 1%) as well as low tensile strength because dislocations are highly mobile at relatively low stress levels [1,10,11]. At present, the relatively large elastic strain limit (exceeding 1%) is only achieved in titanium alloys, nanowires and single crystal or amorphous alloys, but they are difficult to be used as electrical contact materials because of their relatively low conductivity and size limit [12–20].

On the other hand, the polymer-containing conductive materials, usually with higher elastic strain limit than metals, normally display inferior electrical conductivity and low strength, especially at elevated temperatures. Shape memory alloys were regularly taken as a reinforcement phase to fabricate electrical contact composite materials to enhance their elastic performance and strength [21–27]. This is because shape memory alloys with austenite phase present a large range of nonlinear elasticity, essentially attributed to the stress-induced martensitic transformation during loading and the reverse transformation during unloading [28,29]. For instance, the coaxial

* Corresponding authors.
** Corresponding authors at: Shi-Changxu Innovation Center for Advanced Materials, Institute of Metal Research, Chinese Academy of Sciences, Shenyang 110016, China.
E-mail addresses: qin.yu.unr@gmail.com (Q. Yu), wanghm02@sjtu.edu.cn (H. Wang), zengqianliu@imr.ac.cn (Z. Liu), zhfzhang@imr.ac.cn (Z. Zhang).

https://doi.org/10.1016/j.apmt.2022.101639
Received 7 June 2022; Received in revised form 16 August 2022; Accepted 14 September 2022

nitinol-sheath Ag/Cu-core wires fabricated by cold drawn method show a markedly high elastic recoverable strain of ~7% [21,22]. Nevertheless, this method is not suitable for producing bulk-sized materials particularly for electrical contact application. As such, it is intriguing to design bulk-sized electrical contact materials that have an optimized combination of high electrical conductivity, large elasticity, and high mechanical strength.

To this end, here we propose a design strategy encompassing the interpenetrating-phase architecture to fabricate a nitinol (NiTi)-reinforced silver (Ag)-matrix composite. We selected Ag as the matrix material considering its outstanding electrical conductivity [2,21,30]. The austenite NiTi alloy was used as reinforcement phase in view of its superior elasticity and high strength at room and elevated temperatures [31,32]. A two-step process was taken to fabricate the Ag-NiTi composite, which involved sintering of a porous NiTi scaffold and subsequent pressureless infiltration of the Ag melt into the NiTi scaffold. A three-dimensional (3-D) interpenetrating-phase architecture was constructed such that the constituent phases were topologically bi-continuous and mutually interspersed in the composite. The bi-continuous interpenetrating-phase architected Ag-NiTi composite was demonstrated to embrace a good combination of high elastic recoverable strain, high strength, and appealing electrical conductivity.

2. Materials and methods

2.1. Sintering

Spherical NiTi powders (AMC Powders, China) with a median diameter of ~15 μm were used for sintering the NiTi scaffold. NiTi powders were filled in a cylindrical stainless-steel mold having an inner diameter of ~50 mm. By pressing the NiTi powders in the mold under a pressure of 50 MPa for 30 min in ambient air, a cylinder-shaped NiTi scaffold with a diameter of ~50 mm and a height of ~25 mm was obtained. The NiTi scaffold was further contained in a high-purity graphite crucible and sintered at 1000 °C for 60 min inside an SRYL-2300/9 graphite resistance furnace (Jvjing Instrument, China) flowed with inert argon gas.

2.2. Melt infiltration

Small blocks of pure Ag (Shanghai Zhenzi Metals, China) were mechanically burnished and ultrasonically cleaned in acetone together with the NiTi scaffold to remove contamination. The pure Ag blocks were placed on top of the sintered porous NiTi scaffold inside a high-purity graphite crucible. Pressureless Ag infiltration was realized by melting the Ag at 1050 °C (~90 °C higher than its melting point of 962 °C) and subsequently holding for 15 min before cooling within the furnace flowed with inert argon gas. All the specimens were cut from the final infiltrated Ag-NiTi composite block.

2.3. Microstructural characterization

Density of the infiltrated composite was measured using the Archimedes method [33]. The phase constitution was examined by X-ray diffraction (XRD) using an X'Pert-Pro MPD X-ray diffractometer (PANalytical, Netherlands) with Co-K_α radiation working at an accelerating voltage of 40 kV. Scanning electron microscopy (SEM) imaging was conducted using an Inspect F50 field-emission scanning electron microscope (FEI, USA) operating at an accelerating voltage of 20 kV. Image analysis of SEM micrographs was conducted using ImageJ software (NIH, USA) to quantify the volume fractions of the constituent phases. The distribution of elements was measured by energy-dispersive X-ray spectroscopy (EDS) using an Oxford Instruments 7426 spectrometer (Oxford Instruments, UK). The thermal behavior of the composite was characterized by differential scanning calorimetry (DSC) using a Q1000 calorimeter (TA Instruments, USA) with a heating rate of 10 K min^{-1}.

2.4. Electrical conductivity measurement

The electrical conductivity of the composite was measured using a Sigma 2008B current conductivity meter (Xiamen Tianyan Instrument, China). The sample, *i.e.*, Ag-NiTi block, had its diameter and thickness over 20 mm, which far exceeded the diameter of the coil (~10 mm). The measurements were repeated at 6 different locations with a mutual spacing of ~10 mm on the polished surface of the Ag-NiTi block. The value of electrical conductivity was presented in form of mean ± standard deviation.

2.5. Mechanical characterization

Mechanical tests under uniaxial compression and tension were carried out to characterize the mechanical properties of the Ag-NiTi composite. The compression specimens were ground and polished to ~1 μm surface finish, with dimensions of ~4 mm × ~4 mm in cross section and ~8 mm in height. Quasi-static uniaxial compression tests were performed in ambient air with a constant strain rate of 10^{-3} s^{-1}, using an Instron 5982 testing system (Instron, USA). For cyclic compression tests, the samples were loaded and unloaded repeatedly at a fixed strain rate of 10^{-3} s^{-1} such that the peak stress at each cycle had a constant increment of ~60 MPa.

For tensile testing, dog-bone shaped tensile specimens with a gauge length of ~4 mm and cross section of ~1 mm × ~1 mm were prepared by electrical discharge machining, and mechanically polished to ~1 μm surface finish. Quasi-static uniaxial tension tests were performed at a fixed strain rate of 10^{-3} s^{-1} at room temperature using a JEOL MicroTest stage (JEOL, Japan) inside the chamber of a JSM-6510 scanning electron microscope (JEOL, Japan). The specimen surface of the gauge section was *in-situ* monitored by SEM for measuring the tensile strain and characterizing the deformation process. To assess the elastic strain limit, tensile loading-unloading was repeated on a specimen with an increment of the maximum stress at 20 MPa for each cycle. The repeated loading-unloading process was stopped when non-zero residual strain was detected after unloading or microcrack initiation was detected on the specimen surface at a certain stress level during loading, whichever case occurring first. The maximum elastic recoverable strain under tension was obtained as the strain corresponding to the maximum stress prior to the last unloading stroke. For each mechanical testing, at least three specimens were repeated. The results were presented in form of mean ± standard deviation.

For characterization of modulus and hardness in deformed NiTi phase, samples of the composite were compressed to different strains, respectively of 5%, 10%, 20%, and 31% (corresponding to the final fracture of composite), and then unloaded. Nanoindentation tests were performed on the NiTi phase in these samples using an Agilent G200 nanoindenter (Agilent Technologies Inc., USA) with a diamond spherical tip with radius of ~5 μm. The loading and unloading rates were set to be 1 mN/s with a holding time of 10 s at 50 mN. For each sample, 10 random points with a mutual spacing of at least 500 μm were tested.

2.6. Computational simulations

A two-dimensional model of Ag-NiTi composite with dimensions of 100 μm × 100 μm was established using the commercial finite element software ABAQUS (Dassault Systèmes, France). The volume fractions and spatial distributions of Ag and NiTi phases in the numerical model were set in accordance with those extracted from the SEM images. One of the end boundaries of the model (AA') was fixed along the loading direction, *i.e., y* direction. The connection between the two phases was defined with an ideally tight bonding state – that is their deformation was continuous at their boundaries. The compressive force was applied by uniformly distributing the stress on the other boundary (BB'). The simulation of the compressive loading-unloading process was conducted by following such a sequence – that is the model was first compressed to

a strain of 5%, then was unloaded to 0 MPa; subsequently, the model was compressed to a strain of 10% and unloaded to 0 MPa; finally, the model was compressed up to a strain of 12%. Detailed methods of the numerical simulation are further described in Supplementary Materials [34–38]. The material parameters used for simulation are listed in Supplementary Table 1.

3. Results

3.1. Microstructure

Fig. 1 shows the microstructures, element distributions and phase constitutions in the Ag-NiTi 3-D interpenetrating-phase composite. SEM images showed that the open pores in partially sintered NiTi scaffold were filled completely with the Ag phase. No obvious structural flaws, *e.g.*, pores or microcracks, were detected in the infiltrated composite. The two constituent phases were mutually interspersed displaying a bi-continuous nature. Further magnified imaging (inset) indicated no obvious impurity phase in the two constituent phases and their interface (Fig. 1a). EDS measurements confirmed that weak diffusion of elements between the two constituent phases occurred during the infiltration process (Fig. 1b). XRD pattern demonstrated that the composite principally comprised Ag and B2-NiTi (austenite) with no evidence of other phases (Fig. 1c). This was also verified by the DSC results where the austenite finish temperature (A_f) for martensite-to-austenite transformation of the NiTi phase was lower than the room temperature (Supplementary Figure 1). The volume fraction of NiTi phase in the composite was determined to be ~65.4% by analyzing SEM images. The density of the composite was measured to be 7.37 g cm^{-3}, consistent with the value calculated from the rule-of-mixtures, further substantiating the nearly absence of pores in the composite. The electrical conductivity of composite was measured to be 10.43±0.21 MS m^{-1}, which was comparable to those of the majority of conductive metallic materials, *i.e.*, aluminum (Al), copper (Cu), Ag, aurum (Au) and other noble metals and their composites [39–41].

3.2. Mechanical properties

Fig. 2a shows the representative compressive engineering stress-strain curve (black) and the loading-unloading stress-strain curve (red) for the Ag-NiTi 3-D interpenetrating-phase composite. The compressive stress-strain response shows an almost linear elastic behavior up to yielding at 450±66.3 MPa (0.2% offset). After a smooth transition at ~2-3% strain, the material exhibited a high work-hardening rate which was in a range of 0.8-3 GPa (Supplementary Figure 2a). The final failure (shear fracture) of the composite occurred as the compressive strain exceeded ~30%, giving a compressive strength of 1502.6±14.3 MPa. The loading-unloading true stress-strain curves show hysteresis loop characteristics (Supplementary Figure 2a), implying obvious hetero-deformation induced (HDI) hardening effect in the composite during the compression process [42–44]. Such effect can be attributed to the restraint of plastic deformation of Ag phase by NiTi phase and the good elastic-plastic deformation ability of the NiTi phase. The HDI stress was found to exhibit a near linear increasing trend with true strain from ~350 MPa to ~500 MPa at the steady plastic deformation stage with true strains of 2-20% (Supplementary Figure 2b), giving a HDI hardening rate of ~850 MPa. As the strain further increased, the HDI stress decreased because of the interfacial cracking or damaging of the composite.

The stress-strain hysteresis loops resulted from cyclic unloading-reloading also suggest that the composite had a capability to dissipate extra mechanical energy under compressive condition. Specifically, the characteristic energies ($E_{consumed}$, $E_{dissipated}$, and $E_{elastic}$) and the elastic recovery strain (ε_E) associated with a typical loading-unloading-reloading cycle were schematically illustrated in Fig. 2b. Their variations with respect to the total strain are presented in Fig. 2c. As the compressive strain increased, the mechanical energy consumed by irreversible deformation, *e.g.*, plastic deformation in constituent phases and damage at the phase interface, $E_{consumed}$, manifested an initially rapid increase (up to point A) followed by slow increase in the strain of 5-20%. The elastically restored energy, $E_{elastic}$, and viscoelastically dissipated energy, $E_{dissipated}$, displayed similar continuous increase with the total strain. The ε_E exhibited an increasing trend with a continuously decaying slope, reaching a steady level of 1.72±0.13% as the total strain rose to ~15%. The variations of ε_E and $E_{dissipated}$ infer that a pre-compression with a strain over 5% may enhance the composite's capabilities for elastic recovery and energy dissipation under compressive loading condition.

Fig. 2d presents the tensile engineering stress-strain curve (black) up to fracture for the Ag-NiTi composite. The stress-strain response

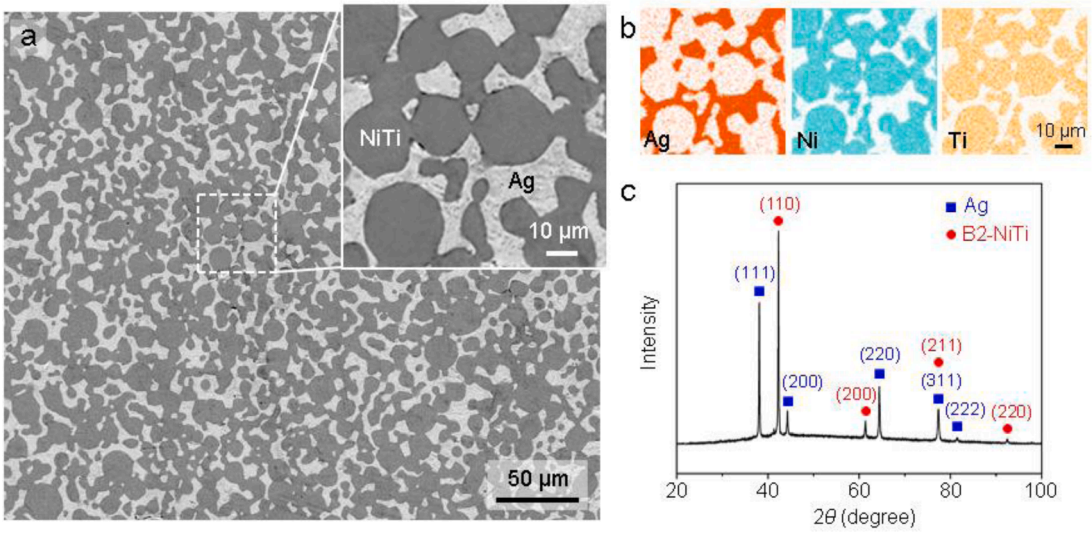

Fig. 1. Microstructure and phase constitution of the Ag-NiTi 3-D interpenetrating-phase composite. (a) SEM images of Ag-NiTi composite. The inset shows the further magnified micrograph of the region indicated by the dashed box. (b) Area distributions of Ag (red), Ni (blue), and Ti (yellow) elements obtained by EDS measurements in the region corresponding to the SEM image in the inset of (a). (c) XRD pattern of the composite. The characteristic diffraction peaks of the crystallographic planes of Ag and B2-NiTi (austenite) phases are indicated on the pattern. (For interpretation of the references to color in this figure legend, the reader is referred to the web version of this article.)

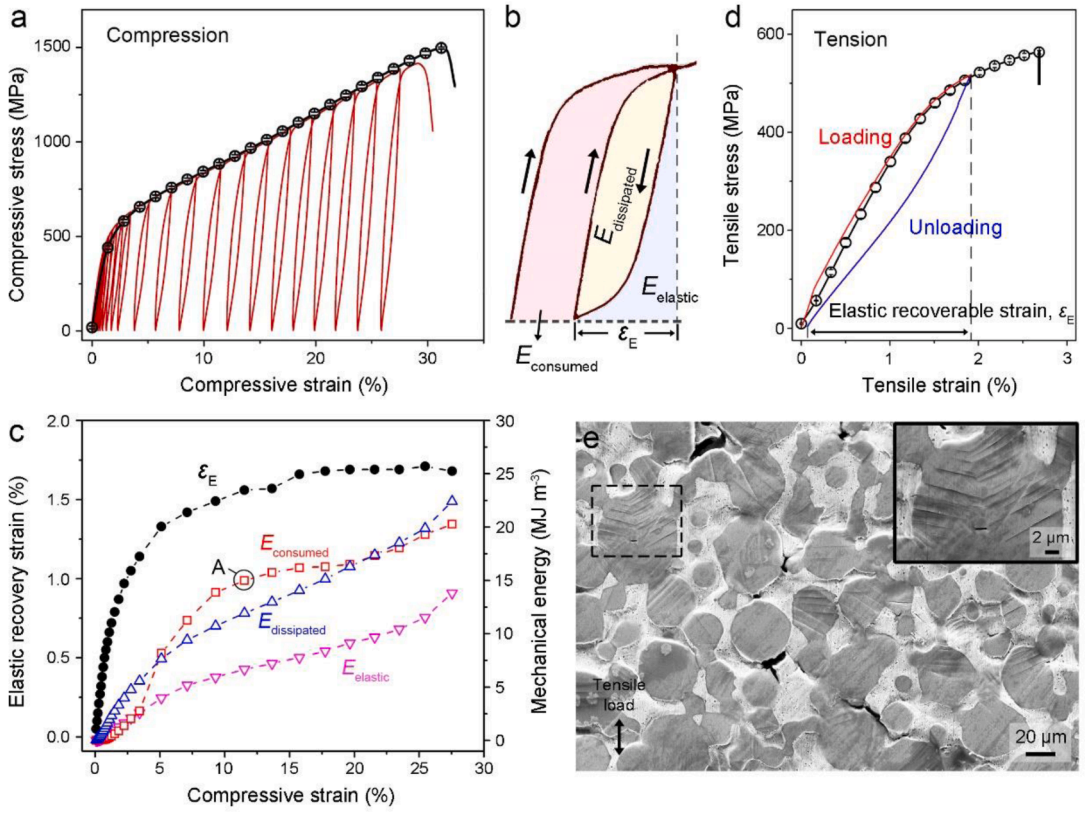

Fig. 2. Ambient-temperature mechanical properties and deformation and damage behavior of the Ag-NiTi 3-D interpenetrating-phase composite. (a) Engineering compressive stress-strain curve (black) and cyclic loading-unloading stress-strain curve (red) of the composite at ambient temperature. (b) Illustrations of the characteristic energies, including the mechanical energy consumed by irreversible deformation $E_{consumed}$, the elastically restored energy $E_{elastic}$, and viscoelastically dissipated energy $E_{dissipated}$, and elastic recovery strain ε_E, under the curves at each loading cycle. (c) Variations of specific energies and elastic recovery strain with the total compressive strain during the cyclic loading-unloading process. A denotes the end of the rapid rising stage of $E_{consumed}$. (d) Engineering tensile stress-strain curve (black) and loading-unloading stress-strain curve (red-blue) of the composite at ambient temperature. The maximum elastic recoverable strain is indicated on the curve. (e) SEM micrograph of deformation and damage morphology in the post-tension specimen for the composite, imaged at the region on the specimen surface near the main fracture plane of the tensile specimen. The inset shows the micrograph of the NiTi phase magnified from the region indicated by the dashed box. (For interpretation of the references to color in this figure legend, the reader is referred to the web version of this article.)

behaved linearly before the material yielded at 372.2±2.2 MPa (0.2% offset). The tensile strength and the elongation to fracture were 564.9 ±6.2 MPa and 2.75±0.05%, respectively. Also shown in Fig. 2d is the loading (red)-unloading (blue) stress-strain curve where microcrack initiation was detected at the peak stress of ~510 MPa corresponding to a strain of ~1.9%. As an almost complete strain recovery was obtained upon unloading from ~510 MPa, the maximum elastic recoverable strain of the composite under tension can be determined to be ~1.71 ±0.06%. This value was close to the saturated elastic recovery strain under compression measured by cyclic loading-unloading experiment. The mechanical properties of the Ag-NiTi composite under both compressive and tensile conditions are listed in Table 1.

Fig. 2e shows the SEM micrographs that captured the featured deformation and damage processes in the post-fracture tensile specimen. Narrow plates of residual martensite were clearly observed in the NiTi phase (inset in Fig. 2e), indicating that martensitic transformation was operated in the NiTi phase and responsible for the large elastic recoverable strain. To verify that martensitic transformation occurred under both tension and compression, we carried out XRD analysis on the specimens fractured under tension and compression. As shown in the XRD patterns of the post-compression and post-tension specimens (Supplementary Figure 3), the characteristic diffraction peaks of B19′-NiTi (martensite) phase were clearly detected under both tension and compression. A higher intensity of B19′-NiTi (martensite) peaks was found in the compression sample due to the much higher stress attained under compression as compared to the tensile sample.

As the elastic strain limit of the Ag phase (<1%) is markedly lower than the phase-transforming strain of the NiTi phase (~6%), the strains are not fully matched between the two phases during the deformation process. Besides the residual martensite plates, interfacial cracking between the NiTi and Ag phases was identified as the major damage of the composite (Fig. 2e). The interfacial cracks propagated limitedly and were confined within the continuous NiTi and Ag phases. This demonstrates that the 3-D interpenetrating-phase architecture is effective in playing roles in the crack arrestment that essentially benefits the damage tolerance of the composite.

The occurrence of martensitic transformation in the NiTi phase during loading can be further verified by examining the deformation process of the composite. As shown in Fig. 3a, plastic deformation preferentially occurred in the Ag phase at small strains and became obvious in the NiTi phase as the strain increased. Diffraction peaks of B19'-NiTi (martensite) phase, which were absent for the undeformed samples, emerged in the XRD patterns of deformed samples and

Table 1
Mechanical properties of Ag-NiTi 3-D interpenetrating-phase composite under compressive and tensile loading conditions.

	Compression	Tension
Yield strength (MPa)	450.8±66.3	372.2±2.2
Ultimate strength (MPa)	1502.6±14.3	564.9±6.2
Elastic recoverable strain (%)	1.72±0.13	1.71±0.06
Fracture strain (%)	31.33±0.29	2.75±0.05

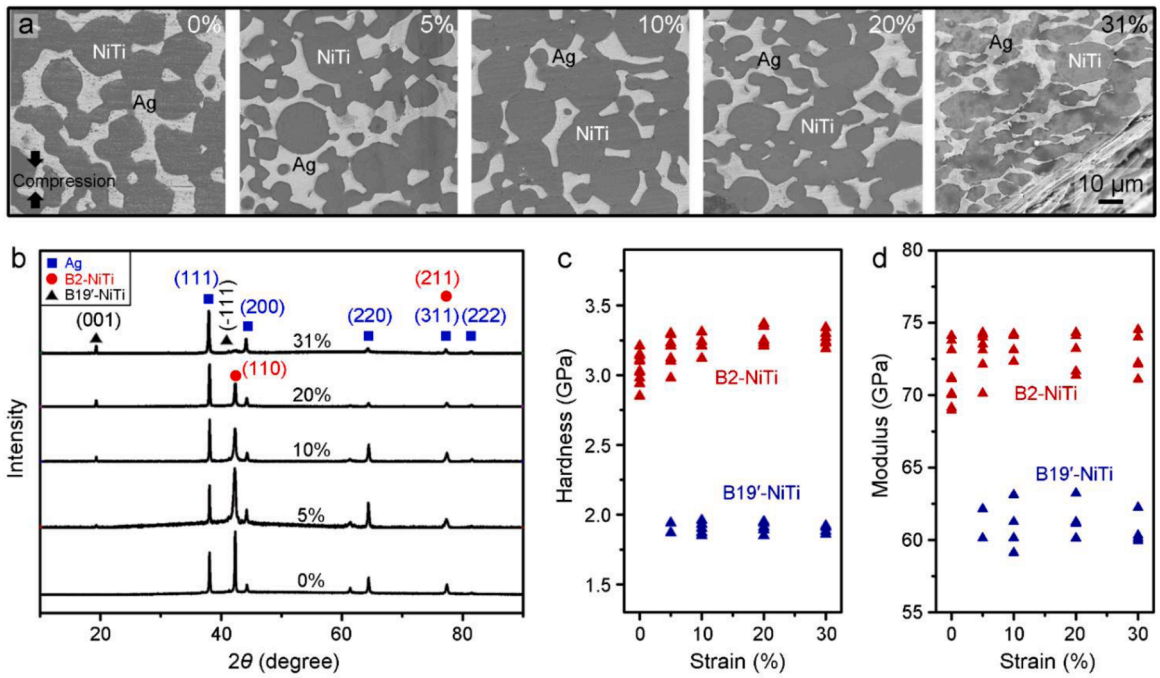

Fig. 3. Compressive deformation process of the Ag-NiTi 3-D interpenetrating-phase composite. (a, b) SEM micrographs and XRD patterns of the Ag-NiTi composite samples subject to different compressive strains of 0%, 5%, 10%, 20%, and 31% (corresponding to the final fracture of the composite). The XRD patterns were adjusted such that the (111) planes of the Ag phase exhibited an identical intensity in all the curves. (c, d) Hardness and elastic modulus of the NiTi phase measured by nanoindentation testing in the composite samples compressed to different strains.

exhibited an increasing intensity with the increase in the compressive strain, as shown in Fig. 3b; at the same time, the relative intensity of diffraction peaks for the B2-NiTi (austenite) phase decreased. Moreover, the hardness and elastic modulus of the NiTi phase measured by nanoindentation testing in undeformed samples were respectively in ranges of 2.8-3.2 GPa and 70-75 GPa (Fig. 3c and d), conforming well to those of the B2-NiTi (austenite) phase reported in literature [45,46]. However, in the deformed composite, lower hardness and modulus of respectively 1.8-2.0 GPa and 59-64 GPa were also detected in specific regions of the NiTi phase in addition to the work-hardening trend of the B2-NiTi. These values are consistent with those reported for the B19'-NiTi (martensite) phase, further validating the occurrence of martensitic transformation [45,46].

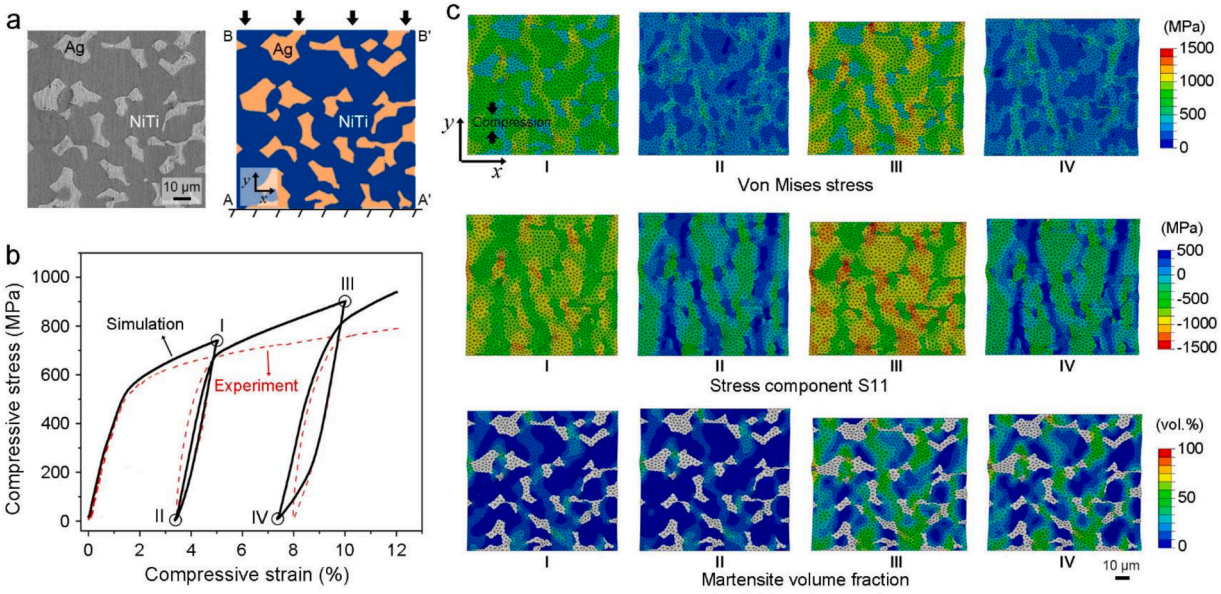

Fig. 4. Computational simulation of the deformation process for the Ag-NiTi 3-D interpenetrating-phase composite. (a) Two-dimensional model employed for FEA simulation for the Ag-NiTi 3-D interpenetrating-phase composite. The model (right) was established in line with the volume fractions and spatial distributions of Ag and NiTi phases characterized by SEM (left). (b) Comparison of cyclic loading-unloading true stress-strain curves between the simulation (solid curve) and experiment (dash curve) results for the composite. I, II, III, and IV denote the four stress transition points. (c) Changes in the effective von Mises stress field, principal stress field S11 along the compressive direction, *i.e., y* axis, and the volume fraction of the martensite phase in the NiTi constituent in the model during loading-unloading process, respectively corresponding to the points I, II, III and IV in (b).

3.3. Deformation mechanisms

To reveal the individual deformation processes of the NiTi and Ag phases in the Ag-NiTi composite underlying repeated compressive loading-unloading cycles, finite element analysis (FEA) simulation was performed by employing a plane-strain composite model that replicated the spatial distributions and volume fractions of Ag and NiTi phases characterized by SEM (Fig. 4a). As shown in Fig. 4b, the simulated stress-strain curve was qualitatively consistent with the experimental result. The distribution maps of von Mises stress, stress component S11 which is the stress component along the compressive direction (*y* axis), and the volume fraction of martensite phase in the NiTi constituent, respectively, at the maximum stresses (points I and III in Fig. 4b) and the minimum stresses (points II and IV in Fig. 4b) of two consecutive loading-unloading cycles are presented in Fig. 4c. As revealed from the von Mises stress distributions at the maximum stresses (points I and III), the bi-continuous interpenetrating-phase architecture enabled an effective load transfer from the Ag to the NiTi phase, thereby alleviating the stress concentration accumulated in the plastically deformed Ag phase during the loading process. As visualized in the distribution map of martensite volume fraction at points I and III, martensitic transformation persisted in the NiTi phase during loading at locations where the internal stress exceeded the critical stress for martensitic transformation which was reported to be around 650 MPa [35,36].

After the external compression was unloaded at points II and IV, the compressive stress in the NiTi phase was partially released due to the constraints of the plastically deformed Ag phase (Supplementary Figure 4), resulting in residual compressive stress. At a majority of regions in the NiTi phase, the magnitude of the residual compressive stress was found to be higher than the stress of 350 MPa for activating martensite-to-austenite transformation [35,36]. This suggests a small portion of the B19′-NiTi (martensite) phase generated during loading was reversely transformed into B2-NiTi (austenite) phase after unloading. This was further confirmed by the slight decrease of the martensite volume fractions between points I and II (or between points III and IV). Interestingly, because of the compressive residual stress in the NiTi phase at the unloading points II and IV, the residual stress in the Ag phase was found to be in tensile state.

4. Discussion

Engineering materials that possess good electrical conductivity as well as high strength and large elastic strain limit have been sought by material scientists particularly for electrical contact application. However, these properties usually exhibit mutually exclusive relationships, such as electrical conductivity *vs.* elasticity and electrical conductivity *vs.* strength. Although attempts have been made to utilize NiTi alloy to make Ag-NiTi wires that show high elastic recoverable strain [21], it remains challenging to fabricate bulk-sized electrical contact materials with good combination of properties of conductivity, strength and elasticity. Here, we demonstrate that good electrical conductivity can be combined with large elastic recoverable strain and high mechanical strength in a bulk-sized Ag-NiTi composite. This is achieved principally by introducing a 3-D bi-continuous interpenetrating-phase architecture through pressureless infiltration of the melted Ag into the partially sintered NiTi scaffold.

As shown in Fig. 5a, our Ag-NiTi interpenetrating-phase composite displays high electrical conductivity which is comparable to those of most metallic materials and superior to carbon materials and polymer conductors [39-41,47-50]. Additionally, the elastic recoverable strain of the Ag-NiTi composite is higher than those of most common bulk-sized conductive metals [1,21,41], making it particularly promising for electrical contact application. It should be noted that compared to the current Ag-NiTi composite, larger elastic strain limit of ~7% has been obtained in hierarchical Ag-NiTi composite wires [21]. This can be attributed to the following three aspects: 1) the NiTi content in the wires (~88 vol.%) is higher than that in the current composite (~65 vol.%); 2) the wires contain less dislocations or defects because of their small (cross-sectional) dimensions and hence exhibit higher strength and elasticity, which is reminiscent of the known Hall-Petch relationship in metals and alloys [16,17,51,52]; 3) the interfaces between the Ag and NiTi phases in the wires are principally parallel to the loading direction, and thereby are more difficult to cracking. Nevertheless, it is much more difficult to achieve large elastic strain limit in bulk-sized materials which are most commonly used for electrical contact application. Furthermore, the ultimate tensile strength of our composite outperforms those of most alloys and composites based on Ag and other noble metals that are used for electrical contact application [39-41,47-50,53-57], as shown in Fig. 5b.

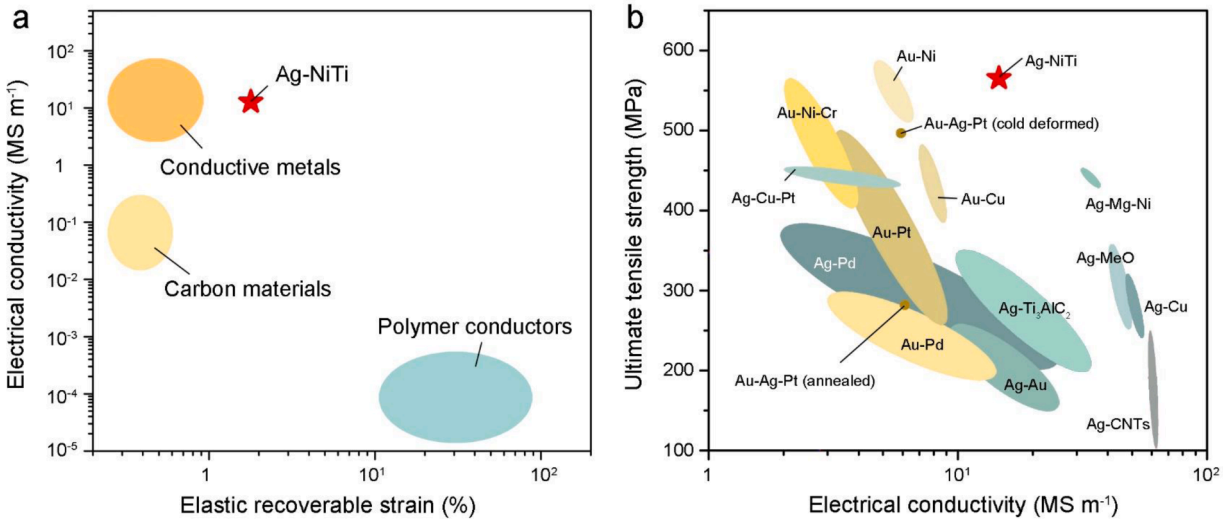

Fig. 5. Comparison of the properties of the Ag-NiTi 3-D interpenetrating-phase composite with other materials at ambient temperature. (a) Electrical conductivity *versus* the elastic recoverable strain for the Ag-NiTi composite, conductive metals (including Al, Cu, Ag, Au and other noble metals and alloys), carbon materials and polymer conductors [1,21,31-39,47-50]. (b) Ultimate tensile strength along with the electrical conductivity of the Ag-NiTi composite, as compared to alloys and composites based on Ag and other noble metals that are commonly used in electrical contact application [39-41,47-50,53-57]. CNT: carbon nanotube; MeO: metal oxides.

The good electrical conductivity of the current bulk-sized Ag-NiTi composite originates from the 3D bi-continuous interpenetrating-phase architecture. Specifically, the continuity of the individual phase (either Ag or NiTi) provides unblocked carrier paths that reduce the electron scattering at phase boundaries and thus promotes the transport efficiency of electrons. The high strength of the composite is derived from the good continuity of the reinforcement NiTi scaffold. The hetero-deformation induced (HDI) hardening effect also plays a role in strengthening the composite [42–44]. On the one hand, geometrically necessary dislocations are generated in the Ag phase and pile up near its interface with NiTi phase, leading to a long-range internal stress [42–44]. On the other hand, as the strain increases, the good elastic-plastic deformation ability of the NiTi phase prevents the premature failure and promotes continuous work-hardening behavior of the two phases. Additionally, the unique martensitic transformation and reverse transformation in the NiTi phase play the key role in the large deformation recovery upon the removal of external load. It deserves to note that the interpenetrating-phase architecture enables effective stress transfer and promotes a synergy of deformation between the constitutive phases, which has been proved in many studies [58–63]. Specifically, the stress concentration in the plastically deformed Ag phase during the loading process can be effectively alleviated through the load share by the NiTi phase (Fig. 4c), which leads to a retardation of material damage in the Ag phase. Moreover, the spread of damage, specifically from plastic deformation in the Ag and cracking at the interface, can be confined by the partition between the two constituent phases. This leads to a controlled damaging process that retards the catastrophic failure and thereby enhances the damage tolerance of the composite.

The mechanical and electrical properties of the Ag-NiTi composite are mainly dependent on three factors: the chemical phase constitution, the composite architecture, and the structure of individual constituent phases. We anticipate that these characteristics can be regulated using the current two-step processing method, thereby enabling the modulation of the properties of composite. For example, the content of Ag phase in the composite can be modulated by adjusting the porosity of the NiTi scaffold before infiltration via controlling the sintering parameters or by adding Ag powders into the NiTi powders during the fabrication of NiTi scaffold. The characteristic dimensions of the composite architecture can also be regulated via adjusting the pore size in the scaffold, which can be realized by controlling the mean diameter of the NiTi powders and the sintering parameters. For example, the decrease of pore size in the NiTi scaffold invariably leads to finer composite structure in the infiltrated Ag-NiTi composite, thereby tends to increase the strength of the composite for given contents of constituent phases [64,65]. It is even possible to regulate the structure of individual constituent phases in the composite, *e.g.*, adjusting the grain size of Ag phase by varying the cooling rate after melt infiltration. Nevertheless, the detailed influences of different factors on the properties of composite remain to be explored in future studies.

5. Conclusions

A new bulk-sized Ag-NiTi 3-D interpenetrating-phase composite has been developed by pressureless infiltration of a partially sintered NiTi scaffold with a Ag melt. The composite exhibits good electrical conductivity and maintains a high mechanical strength along with a large elastic recoverable strain, exceeding most of the bulk metallic materials. The good electrical conductivity arises from the continuous nature of the Ag phase that promotes the transport efficiency of electrons. The NiTi scaffold which is also continuous not only enhances the strength of the composite but also improves the elastic recovery through the reversible stress-induced austinite-martensite transformation characteristic of NiTi phase. In addition, the 3-D interpenetrating-phase architecture functions to confine the spread of damages in the constituents and at the interfaces, promoting the composite's damage tolerance and strengthening capability. The combination of good electrical conductivity, large elasticity and high strength in the bulk Ag-NiTi composite makes the material a promising candidate for electrical contact application.

Data availability

The data that support the findings of this study are available from the corresponding author, Prof. Zengqian Liu, at zengqianliu@imr.ac.cn, upon reasonable request.

Author contributions

Z.L., Q.Y. and Z.Z. designed the research; J.Z. and F.W. fabricated the composites; M.Z. and Y.Z. characterized the microstructures and measured the mechanical properties; H.W. implemented the computational simulations; M.Z., Z.L., Q.Y., H.W., D.X., Z.Z. and R.O.R. analyzed and discussed the data; M.Z., Z.L. and Q.Y. wrote the initial paper; Z.Z. and R.O.R. revised the paper.

Declaration of Competing Interest

The authors declare no conflict of interest.

Acknowledgements

The authors are grateful for the financial support by the National Key R&D Program of China [grant number 2020YFA0710404]; the National Natural Science Foundation of China [grant numbers 51871216, 52173269]; the KC Wong Education Foundation [grant number GJTD-2020-09]; the Liaoning Revitalization Talents Program, and the Youth Innovation Promotion Association CAS [grant number 2019191]. ROR was supported by the Multi-University Research Initiative [grant number AFOSR-FA9550-15-1-0009] from the Air Force Office of Scientific Research.

References

[1] S. Hao, L. Cui, D. Jiang, X. Han, Y. Ren, J. Jiang, Y. Liu, Z. Liu, S. Mao, Y. Wang, Y. Li, X. Ren, X. Ding, S. Wang, C. Yu, X. Shi, M. Du, F. Yang, Y. Zheng, Z. Zhang, X. Li, D.E. Brown, J. Li, A transforming metal nanocomposite with large elastic strain, low modulus, and high strength, Science 339 (2013) 1191–1194.
[2] F. Findik, H. Uzun, Microstructure, hardness and electrical properties of silver-based refractory contact materials, Mater. Design 24 (2003) 489–492.
[3] M. Chin, J.R. Barber, S.J. Hu, Effect of elastic recovery on the electrical contact resistance in anisotropic conductive adhesive assemblies, IEEE Trans. Compon. Packaging Technol. 29 (2006) 137–144.
[4] L. Kogut, K. Komvopoulos, Electrical contact resistance theory for conductive rough surfaces, J. Appl. Phys. 94 (2003) 3153–3162.
[5] M. Chin, K.A. Iyer, S.J. Hu, Prediction of electrical contact resistance for anisotropic conductive adhesive assemblies, IEEE Trans. Compon. Packaging Technol. 27 (2004) 317–326.
[6] G.C. Kuczynski, Effect of elastic strain on the electrical resistance of metals, Phys. Rev. 94 (1954) 61–64.
[7] M. Ciavarella, V. Delfine, G. Demelio, A "re-vitalized" Greenwood and Williamson model of elastic contact between fractal surfaces, J. Mech. Phys. Solids 54 (2006) 2569–2591.
[8] P.V. Andrews, M.B. West, C.R. Robeson, The effect of grain boundaries on the electrical resistivity of polycrystalline copper and aluminium, Philos. Mag. 19 (1969) 887–898.
[9] L. Lu, Y. Shen, X. Chen, L. Qian, K. Lu, Ultrahigh strength and high electrical conductivity in copper, Science 304 (2004) 422–426.
[10] T. Zhu, J. Li, Ultra-strength materials, Prog. Mater. Sci. 55 (2010) 710–757.
[11] Z. Chen, H.J. Bong, D. Li, R.H. Wagoner, The elastic-plastic transition of metals, Int. J. Plast. 83 (2016) 178–201.
[12] S. Kuramoto, T. Furuta, J. Hwang, K. Nishino, T. Saito, Elastic properties of Gum Metal, Mater. Sci. Eng. A-Struct. 442 (2006) 454–457.
[13] T. Saito, T. Furuta, J.H. Hwang, S. Kuramoto, K. Nishino, N. Suzuki, R. Chen, A. Yamada, K. Ito, Y. Seno, T. Nonaka, H. Ikehata, N. Nagasako, C. Iwamoto, Y. Ikuhara, T. Sakuma, Multifunctional alloys obtained via a dislocation-free plastic deformation mechanism, Science 300 (2003) 464–467.
[14] E.G. Obbard, Y.L. Hao, R.J. Talling, S.J. Li, Y.W. Zhang, D. Dye, R. Yang, The effect of oxygen on α″ martensite and superelasticity in Ti–24Nb–4Zr–8Sn, Acta Mater. 59 (2011) 112–125.
[15] T. Fukuda, T. Kakeshita, More than 6% elastic strain realized in a bulk single crystal of an Fe_3Pt alloy, Scr. Mater. 69 (2013) 89–91.

[16] Y. Yue, P. Liu, Z. Zhang, X. Han, E. Ma, Approaching the theoretical elastic strain limit in copper nanowires, Nano Lett. 11 (2011) 3151–3155.
[17] H. Zhang, J. Tersoff, S. Xu, H. Chen, Q. Zhang, K. Zhang, Y. Yang, C.S. Lee, K.N. Tu, J. Li, Y. Lu, Approaching the ideal elastic strain limit in silicon nanowires, Sci. Adv. 2 (2016), e1501382.
[18] L. Tian, Y.Q. Cheng, Z.W. Shan, J. Li, C.C. Wang, X.D. Han, J. Sun, E. Ma, Approaching the ideal elastic limit of metallic glasses, Nat. Commun. 3 (2012) 609.
[19] W.L. Johnson, Bulk amorphous metal – an emerging engineering material, JOM 54 (2002) 40–43.
[20] D.C. Hofmann, J.Y. Suh, A. Wiest, G. Duan, M.L. Lind, M.D. Demetriou, W. L. Johnson, Designing metallic glass matrix composites with high toughness and tensile ductility, Nature 451 (2008) 1085–1089.
[21] S. Hao, L. Cui, J. Jiang, F. Guo, X. Xiao, D. Jiang, C. Yu, Z. Chen, H. Zhou, Y. Wang, Y. Liu, D.E. Brown, Y. Ren, A novel multifunctional NiTi/Ag hierarchical composite, Sci. Rep. 4 (2014) 5267.
[22] S. Hao, L. Cui, Z. Chen, D. Jiang, Y. Shao, J. Jiang, M. Du, Y. Wang, D.E. Brown, Y. Ren, A novel stretchable coaxial NiTi-sheath/Cu-core composite with high strength and high conductivity, Adv. Mater. 25 (2012) 1199–1202.
[23] O. Fouassier, J. Chazelas, J.F. Silvain, Conception of a consumable copper reaction zone for a NiTi/SnAgCu composite material, Compos. Part A-Appl. Sci. Manuf. 33 (2002) 1391–1395.
[24] M. Dulski, J. Balcerzak, W. Simka, K. Dudek, Innovative bioactive Ag-SiO_2/TiO_2 coating on a NiTi shape memory alloy: structure and mechanism of its formation, Materials 14 (2021) 99.
[25] J. Zhang, Y. Liu, L. Cui, S. Hao, D. Jiang, K. Yu, S. Mao, Y. Ren, H. Yang, Lattice strain matching"-enabled nanocomposite design to harness the exceptional mechanical properties of nanomaterials in bulk forms, Adv. Mater. 32 (2020), 1904387.
[26] S. Wang, L. Cui, S. Hao, D. Jiang, Y. Liu, Z. Liu, S. Mao, X. Han, Y. Ren, Locality and rapidity of the ultra-large elastic deformation of Nb nanowires in a NiTi phase-transforming matrix, Sci. Rep. 4 (2014) 6753.
[27] X. Kong, Y. Yang, Z. Sun, H. Yang, Y. Liu, Y. Ren, L. Cui, C. Chen, S. Hao, *In-situ* high energy X-ray diffraction study of microscopic deformation behavior of martensite variant reorientation in NiTi wire, Appl. Mater. Today 22 (2021), 100904.
[28] G. Tan, Y. Liu, Comparative study of deformation-induced martensite stabilisation via martensite reorientation and stress-induced martensitic transformation in NiTi, Intermetallics 12 (2004) 373–381.
[29] L. Orgéas, D. Favier, Stress-induced martensitic transformation of a NiTi alloy in isothermal shear, tension and compression, Acta Mater. 46 (1998) 5579–5591.
[30] G. Li, T. Yang, Y. Ma, W. Feng, X. Zhang, X. Fang, Mechanical characteristics of the Ag/SnO_2 electrical contact materials with Cu_2O and CuO additives, J. Alloy. Compd. 817 (2020), 152710.
[31] D.S. Li, X.P. Zhang, Z.P. Xiong, Y.W. Mai, Lightweight NiTi shape memory alloy based composites with high damping capacity and high strength, J. Alloy. Compd. 490 (2010) L15–L19.
[32] K. Neuking, A. Abu-Zarifa, S. Youcheu-Kemtchou, G. Eggeler, Polymer/NiTi-composites: fundamental aspects, processing and properties, Adv. Eng. Mater. 7 (2005) 1014–1023.
[33] S.W. Hughes, Archimedes revisited: a faster, better, cheaper method of accurately measuring the volume of small objects, Phys. Educ. 40 (2005) 468–474.
[34] D. Cho, J.H. Kim, H.C. Kwon, K.H. Kim, Strain hardening characteristics of 99.9% pure silver at large strains, Int. J. Precis. Eng. Manuf. 22 (2021) 1061–1067.
[35] W.W. Chen, Q.P. Wu, J.H. Kang, N.A. Winfree, Compressive superelastic behavior of a NiTi shape memory alloy at strain rates of 0.001-750 s^{-1}, Int. J. Solids Struct. 38 (2001) 8989–8998.
[36] X. Huang, Y. Liu, Effect of annealing on the transformation behavior and superelasticity of NiTi shape memory alloy, Scr. Mater. 45 (2001) 153–160.
[37] F. Auricchio, R.L. Taylor, Shape-memory alloys: modelling and numerical simulations of the finite-strain superelastic behavior, Comput. Methods Appl. Mech. Eng. 143 (1997) 175–194.
[38] D.C. Drucker, W. Prager, Soil mechanics and plastic analysis for limit design, Q. Appl. Math. 10 (1952) 157–165.
[39] B.B. Zhang, N.R. Tao, K. Lu, A high strength and high electrical conductivity bulk Cu-Ag alloy strengthened with nanotwins, Scr. Mater. 129 (2017) 39–43.
[40] H.Y. Yang, Z.C. Ma, C.H. Lei, L. Meng, Y.T. Fang, J.B. Liu, H.T. Wang, High strength and high conductivity Cu alloys: a review, Sci. China Tech. Sci 63 (2020) 2505–2517.
[41] M.F. Ashby, Materials Section in Mechanical Design, third ed., Pergamon Press, Oxford, 2005.
[42] Y. Zhu, X. Wu, Perspective on hetero-deformation induced (HDI) hardening and back stress, Mater. Res. Lett. 7 (2019) 393–398.
[43] X.T. Fang, G.Z. He, C. Zheng, X.L. Ma, D. Kaoumi, Y.S. Li, Y.T. Zhu, Effect of heterostructure and hetero-deformation induced hardening on the strength and ductility of brass, Acta Mater. 186 (2020) 644–655.
[44] X. Wu, M. Yang, F. Yuan, G. Wu, Y. Wei, X. Huang, Y. Zhu, Heterogeneous lamella structure unites ultrafine-grain strength with coarse-grain ductility, Proc. Natl. Acad. Sci. USA 112 (2015) 14501–14505.
[45] W. Yan, A. Amini, Q. Sun, On anomalous depth-dependency of the hardness of NiTi shape memory alloys in spherical nanoindentation, J. Mater. Res. 28 (2013) 2031–2039.
[46] M. Kabla, D. Shilo, Characterization of NiTi superelastic properties by nano-dynamic modulus analysis and nanoindentation, Funct. Mater. Lett. 10 (2017), 1650071.
[47] S. Pan, T. Wang, K. Jin, X. Cai, Understanding and designing metal matrix nanocomposites with high electrical conductivity: a review, Comput. Methods Appl. Mech. Eng. 57 (2022) 6487–6523.
[48] D. Kumar, R.C. Sharma, Advances in conductive polymers, Eur. Polym. J. 34 (1998) 1053–1060.
[49] D.D.L. Chung, Electrical applications of carbon materials, J. Mater. Sci. 39 (2004) 2645–2661.
[50] W. Zhang, A.A. Dehghani-Sanij, R.S. Blackburn, Carbon based conductive polymer composites, J. Mater. Sci. 42 (2007) 3408–3418.
[51] E.O. Hall, The deformation and ageing of mild steel: III discussion of results, Proc. Phys. Soc. B. 64 (1951) 747.
[52] N.J. Petch, The cleavage strength of polycrystals, J. Iron Steel Inst. 174 (1953) 25–28.
[53] Y. Yang, Y. Ping, Y. Gong, Z. Wang, Q. Fu, C. Pan, Ag/graphene composite based on high-quality graphene with high electrical and mechanical properties, Prog. Nat. Sci. 29 (2019) 384–389.
[54] C. Zhao, X. Zuo, E. Wang, R. Niu, K. Han, Simultaneously increasing strength and electrical conductivity in nanostructured Cu-Ag composite, Mater. Sci. Eng. A-Struct. 652 (2016) 296–304.
[55] M. Liu, J. Chen, H. Cui, X. Sun, S. Liu, M. Xie, Ag/Ti3AlC2 composites with high hardness, high strength and high conductivity, Mater. Lett 213 (2018) 269–273.
[56] D. Jia, J. Ma, X. Gan, J. Tao, M. Xie, J. Yi, Y. Liu, A comparison study of Ag composites prepared by spark plasma sintering and hot pressing with silver-coated CNTs as the reinforcements, Materials 12 (2019) 1949.
[57] C.P. Wu, D.Q. Yi, W. Weng, S.H. Li, J.M. Zhou, Influence of alloy components on arc erosion morphology of Ag/MeO electrical contact materials, Trans. Nonferrous Met. Soc. China 26 (2016) 185–195.
[58] M. Zhang, Q. Yu, Z. Liu, J. Zhang, G. Tan, D. Jiao, W. Zhu, S. Li, Z. Zhang, R. Yang, R.O. Ritchie, 3D printed Mg-NiTi interpenetrating-phase composites with high strength, damping capacity, and energy absorption efficiency, Sci. Adv. 6 (2020) eaba5581.
[59] P. Chen, C. Kenel, Y. Wang, D.C. Dunand, SnO2-Ag composites with high thermal cycling stability created by Ag infiltration of 3D ink-extruded SnO2 microlattices, Appl. Mater. Today 21 (2020), 100794.
[60] Z. Jia, L. Wang, 3D printing of biomimetic composites with improved fracture toughness, Acta Mater. 173 (2019) 61–73.
[61] L. Wang, J. Lau, E.L. Thomas, M.C. Boyce, Co-continuous composite materials for stiffness, strength, and energy dissipation, Adv. Mater. 23 (2011) 1524–1529.
[62] L. Wang, S. Wu, X. Guo, J. Fan, S. Zhou, Z. Chen, Multi-shape-changing interpenetrating networks with shape memory effect and adaptive plastic deformations, Appl. Mater. Today 25 (2021), 101246.
[63] J.H. Lee, L. Wang, M.C. Boyce, E.L. Thomas, Periodic bicontinuous composites for high specific energy absorption, Nano Lett. 12 (2012) 4392–4396.
[64] S. Jiang, L.J. Huang, Q. An, L. Geng, X.J. Wang, S. Wang, Study on titanium-magnesium composites with bicontinuous structure fabricated by powder metallurgy and ultrasonic infiltration, J. Mech. Behav. Biomed. Mater. 81 (2018) 10–15.
[65] Z. Fan, B. Zhang, Y. Gao, X. Guan, P. Xu, Deformation mechanisms of spherical cell porous aluminum under quasi-static compression, Scr. Mater. 142 (2018) 32–35.